## Supplementary Materials

## Experimental Procedures

### Molecular Biology:

To generate the *UAS-PAR-1 RNAi* construct, the primer pair
5'gatcgaattcggttcgcctaacatgcaaatgcggag 3' and
5'gatcgcggccgcctgtggggataagcggtttggtttag 3' were used to amplify an intron-containing *par-1* DNA fragment from genomic DNA and primer pair
5'gatcctcgagggttcgcctaacatgcaaatg-cggag 3' and
5'gatcgcggccgcctatatttgcctctgagcacgcgttc 3' were used to amplify a corresponding cDNA fragment from *par-1* full-length cDNA. The PCR products were digested with the corresponding restriction enzymes for the restriction sites appended at the end of primer sequences. An inverted repeat of gDNA-cDNA was formed by ligating the two digested PCR products and the hybrid fragment was subsequently cloned into the *pUAST* vector.

### *In vitro* phosphorylation assay

The GUK domains of wild-type Dlg and Dlg(S797A) mutant were subcloned into *pGEX 6P-1* vector. The GST-fusion proteins were purified using glutathione agarose matrix according to manufacture's instructions. The resulting purified GST-GUK and GST-GUK(S797A) proteins were subjected to *in vitro* phosphorylation assays. As a source of active PAR-1 kinase, we used the immunoprecipitation approach to isolate active PAR-1 kinase from embryonic or larval protein extracts, which was used in *in vitro* kinase assays as described (Nishimura et al., 2004).

**Immunocytochemistry**

Late third instar larval muscle walls were dissected in $Ca^{2+}$ saline and then fixed in Bouin's fixative for about 30 minutes. The primary antibodies used were: anti-Dlg (Parnas et al., 2001) (1:500, Hybridoma Bank, University of Iowa); anti-CSP (Zinsmaier et al., 1994) (1:20, Hybridoma Bank, University of Iowa); anti-GluRII-A (DiAntonio et al., 1999) (1:20, Hybridoma Bank, University of Iowa); Goat anti-HRP conjugated with TxRed (1:200, Molecular Probes); anti-PAR-1 (Sun et al., 2001; 1:100); Rabbit anti-phospho-Dlg (1:200, raised against the PDKFGpSCVPHT peptide sequence). The corresponding secondary antibodies conjugated with various fluorophores such as Alexa 488nm/Alexa 568nm (Molecular Probes), FITC/TxRed and Cy3/Cy5 (Jackson ImmunoResearch Laboratory) were used for single or double labelling experiments. Confocal images were collected from a Carl Zeiss LSM Meta 150 microscope with a 40x inverted NX 1.4 oil lens. To compare the synaptic and extrasynaptic immunofluorescence intensities, confocal images were collected under identical settings for the various genotypes. Fluorescence intensity quantification was performed using the image analysis package provided for Carl Zeiss LSM Meta 510. To assess bouton formation, the NMJ terminals innervating muscle 6 and 7 at abdominal segment 2 were chosen for quantitative analysis.

**Electron Microscopy**

Electron microcopy analysis was performed essentially as described before (Lahey et al., 1994). The midline cross-sections of type Ib boutons at muscle 6/7 of abdominal segment 2 were selected for the following morphometric analysis: To calculate the number of SSR segments, four lines intersecting at right angles were traced from the center of a bouton

cross- section. The number of SSR segments crossed by each line was scored and averaged. To calculate SSR area vs. bouton area ratio, the domains occupied by SSR and bouton were first traced with sealed circles. Then the area values of SSR and bouton are calculated using NIH image software. The area ratio between SSR and bouton indicates the extent of SSR growth. To quantify synaptic vesicle density, the number of synaptic vesicle was counted and then divided by the cross-section area. Active zones were scored by counting electron dense areas on the presynaptic membrane that frequently contain T-bars, the presumptive sites of neurotransmitter release.

**Electrophysiology**

Electrophysiological recordings of two-electrode voltage-clamp were performed as described (Guo and Zhong, 2006). Recordings were done in haemolymph-like (HL-3) solution containing (in mM): NaCl, 70; KCl, 5; $MgCl_2$, 4; NaHCO3, 10; Trehalose, 5; HEPES, 5; Sucrose, 115, and $Ca^{2+}$, 0.60. All recordings were made at the longitudinal muscles 12 and 6 of segments A3-A5. To elicit EJCs, the segmental nerves were stimulated (Master-8 stimulator, A.M.P.I., Jerusalem, Israel) at 1.5 times the stimulus voltage required for a threshold response. Current signals were amplified with an Axoclamp 2A amplifier (Axon Instruments, Foster City, California), converted to a digital signal using a Digidata 1320A interface (Axon Instruments), and acquired by pClamp 8.0 software (Axon Instruments). Evoked and spontaneous responses were analyzed using the Mini Analysis Program (Synaptosoft Inc., Decatur, GA). Miniature EJCs (mEJCs) within continuous recordings of 1 min (the first 1 min) were taken for analysis. Quantal amplitude (quantal size, *q*) was determined using either the "Gaussian"

fitting (for a single peak) or the "10 Simplex" fitting functions in the Origin program (OriginLabs, Southampton, MA).

**FRAP**

To create a microenvironment saturated with evaporated ether, an ether-soaked paper pad was placed into a capped petri dish. Live third instar larvae were quickly put into the dish. The animals were subjected to ether exposure for 30-45 seconds. Transiently immobilized animals were mounted onto a long, 0.15 mm-thick cover glass for FRAP analysis. We focused on the distal synaptic boutons at muscle 12, one of muscle fibers closest to the white cuticle. Photobleaching was performed according to instructions provided for Carl Zeiss LSM Meta 510. At each time point, an image was collected as a single optical section. The fluorescence intensities were compared and quantified using image J and the image browser supplied for Carl Zeiss LSM Meta 510.

**References:**

DiAntonio, A., Petersen, S. A., Heckmann, M., and Goodman, C. S. (1999). Glutamate receptor expression regulates quantal size and quantal content at the Drosophila neuromuscular junction. J Neurosci *19*, 3023-3032.

Guo, H. F., and Zhong, Y. (2006). Requirement of Akt to mediate long-term synaptic depression in Drosophila. J Neurosci *26*, 4004-4014.

Lahey, T., Gorczyca, M., Jia, X. X., and Budnik, V. (1994). The Drosophila tumor suppressor gene dlg is required for normal synaptic bouton structure. Neuron *13*, 823-835.

Parnas, D., Haghighi, A. P., Fetter, R. D., Kim, S. W., and Goodman, C. S. (2001). Regulation of postsynaptic structure and protein localization by the Rho-type guanine nucleotide exchange factor dPix. Neuron *32*, 415-424.

Sun, T. Q., Lu, B., Feng, J. J., Reinhard, C., Jan, Y. N., Fantl, W. J., and Williams, L. T. (2001). PAR-1 is a Dishevelled-associated kinase and a positive regulator of Wnt signalling. Nat Cell Biol *3*, 628-636.

Zinsmaier, K. E., Eberle, K. K., Buchner, E., Walter, N., and Benzer, S. (1994). Paralysis and early death in cysteine string protein mutants of Drosophila. Science *263*, 977-980.

**Supplementary Figures and Legends**

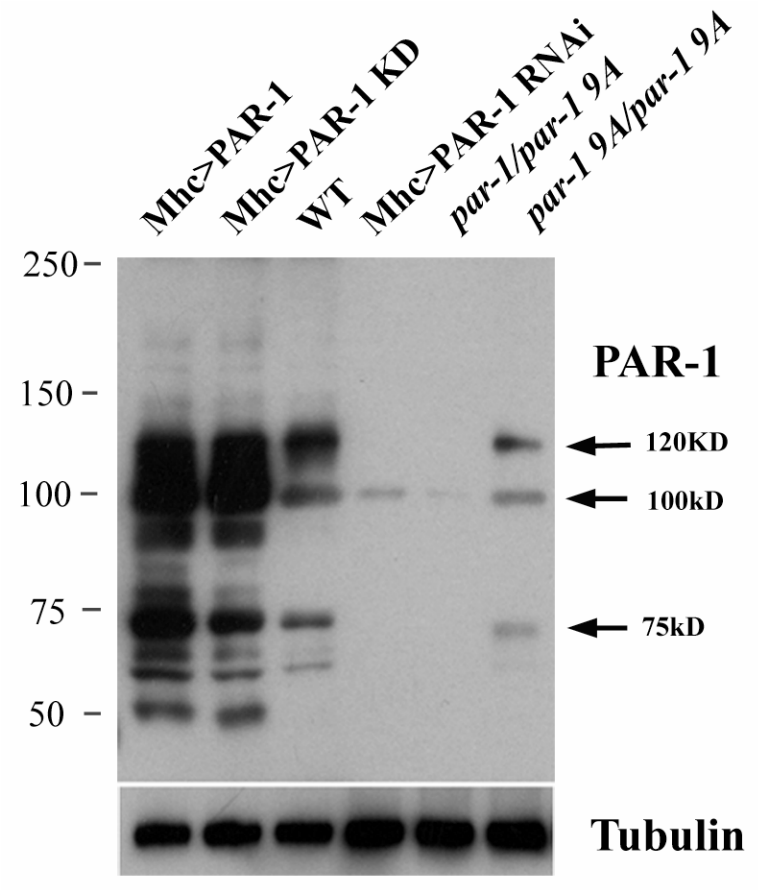


**Figure S1**.Western blot analysis of PAR-1 protein levels in wild type, *Mhc>PAR-1*, *Mhc>PAR-1 KD*, *Mhc>PAR-1 RNAi*, *par-1*$^{9A}$*/par-1*$^{\Delta 16}$, and *par-1*$^{9A}$*/par-1*$^{9A}$ NMJs. Body-wall muscle protein extracts prepared from the above genotypes were separated by SDS-PAGE gel electrophoresis and then subjected to Western blot analysis using an anti-PAR-1 antibody. In wild type extract, there were three major bands (marked by arrows) running at around 75, 100, and 120 kD positions. In both *Mhc>PAR-1* and *Mhc>PAR-1-KD* animals, overexpressing PAR-1 at the postsynapse caused a dramatic increase in the levels of these three protein bands. In contrast, in *par-1*$^{9A}$*/par-1*$^{\Delta 16}$ mutant and *Mhc>PAR-1 RNAi* animals, these PAR-1 protein bands were barely detectable. In the hypomorphic *par-1*$^{9A}$*/par-1*$^{9A}$ animals, PAR-1 protein levels were decreased to a lesser degree.

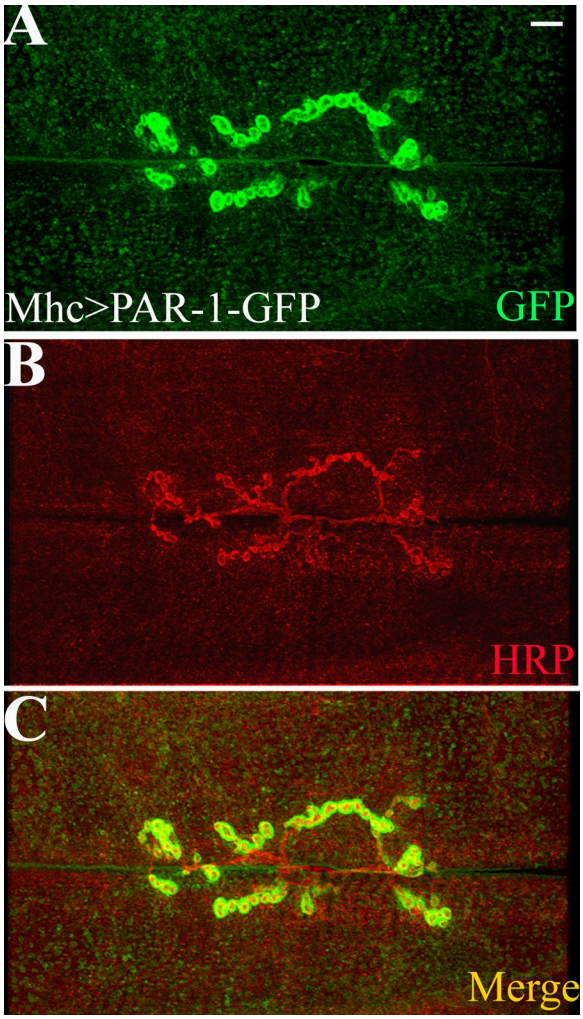


**Figure S2**. Localization of PAR-1-GFP to the postsynapse. Larval NMJ of *Mhc>PAR-1-GFP* animals was double immunostained for GFP (A) and HRP (B). The merged image was shown in C. When the GFP tagged PAR-1 was misexpressed in the postsynaptic muscle cell, it was preferentially localized to the synapse (n=21). Scale bar: 5 μm.

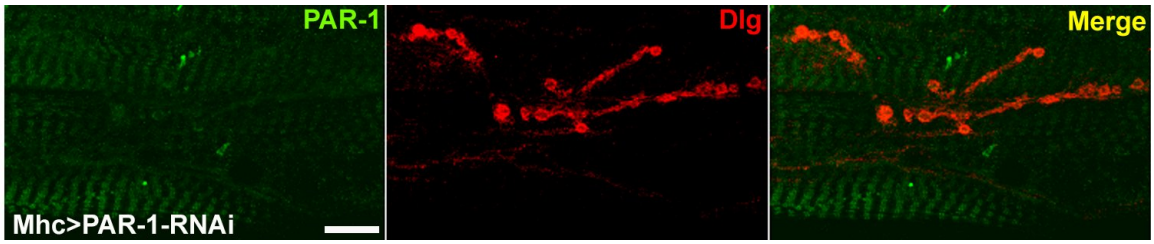


**Figure S3**. Knockdown of PAR-1 protein expression by RNAi. Larval NMJ of *Mhc>PAR-1* RNAi was double stained for PAR-1 (green) and Dlg (red). The merged image was shown on the right. Note that the synaptic anti-PAR-1 signals was dramatically decreased after PAR-1 RNAi. Scale bar: 5 μm.

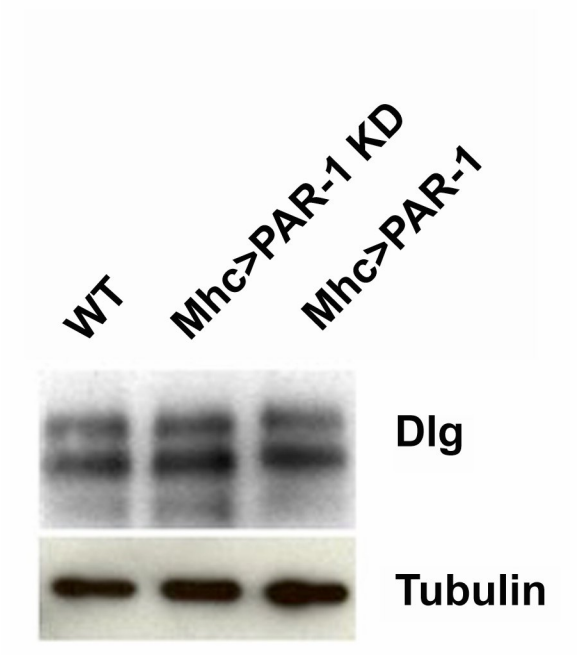


**Figure S4**. Western blot analysis showing comparable Dlg protein expression in wild type, *Mhc>PAR-1*, and *Mhc>PAR-KD* animals. Endogenous Dlg proteins were detected by Western blot analysis with an anti-Dlg antibody. Tubulin serves as a loading control.

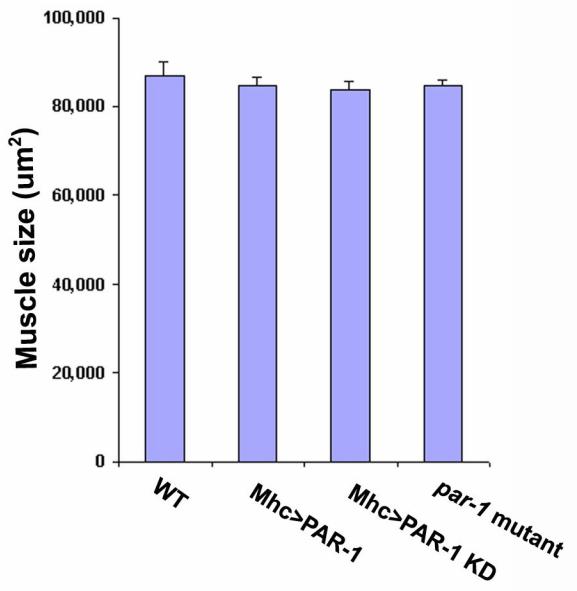


**Figure S5**. Quantitative analysis of the sizes of muscle 6/7 of abdominal segment 2 in wild type (n=30), *Mhc>PAR-1* (n=35), *Mhc>PAR-1-KD* (n=29), and *par-1* mutant (n=32) animals. No significant difference between wild type and PAR-1 loss of function or overexpression animals was found.

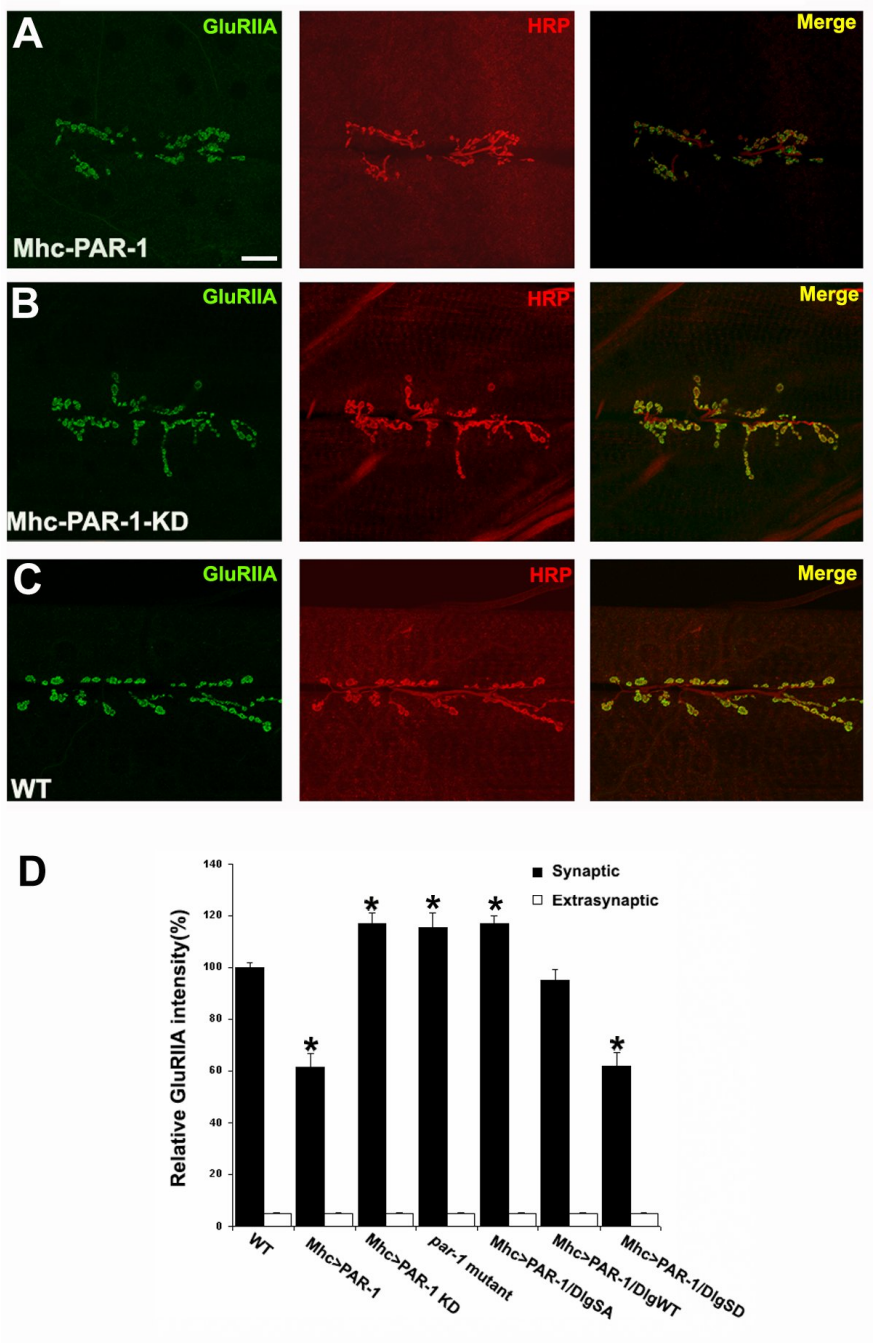


**Figure S6**. Analysis of the effects of PAR-1 on the synaptic localization of GluRIIA.

(A-C) Larval NMJs of *Mhc>PAR-1* (A), *Mhc>PAR-1 KD* (B), and wild type (C) animals were double labelled with anti-GluRIIA (green) and anti-HRP (red). The merged images are shown to the right. Although the intensity of synaptic GluRIIA level was moderately

decreased in *Mhc>PAR-1*, the relative distribution of GluRIIA was not changed, with the protein still being predominantly localized to the postsynapse. Scale bar: 5 μm.

(D) Statistical analysis of the effect of altered PAR-1 activities on GluRIIA localization. Compared to that in wild type animals, the intensity of synaptic GluRIIA was reduced in *Mhc>PAR-1* (n=30, P<0.001) animals, whereas in *par-1* mutant (n=22), *Mhc>PAR-1 KD* (n=25), or *Mhc>PAR-1/DlgSA-GFP* (n=26) animals, the intensity of synaptic GluRIIA was moderately increased (P<0.01). DlgWT-GFP restored synaptic GluRIIA level to normal in *Mhc>PAR-1* background (n=20), while DlgSD-GFP (n=28) has little effect. The level of extrasynaptic GluRIIA was basal and not significantly changed in all the genotypes analyzed.

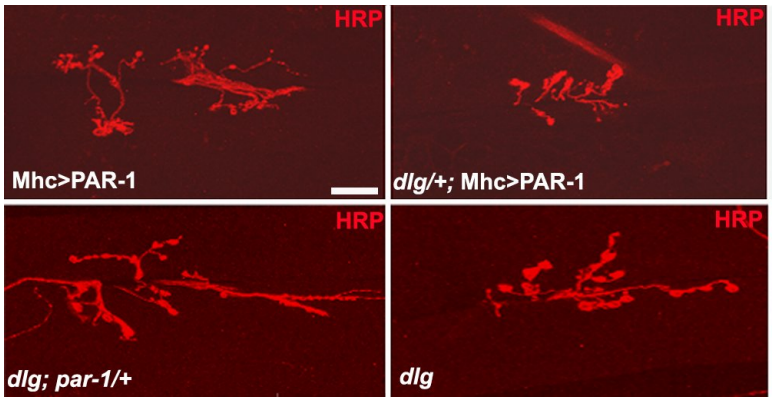


**Figure S7**. Genetic interaction between Dlg and PAR-1. The NMJ terminals of the indicated genotypes were highlighted by anti-HRP immunostaining. Note that removal of one copy of *dlg* exacerbated *Mhc>PAR-1* phenotype, whereas removal of one copy of *par-1* in *dlg* mutant background partially suppressed *dlg* mutant phenotype. Scale bar: 5 μm. Quantification of the data is shown in Figure 2G. The NMJ terminals of *dlg/+* and *par-1/+* animals are normal and similar to the controls shown in Figure 1C2 and Figure 2B2.

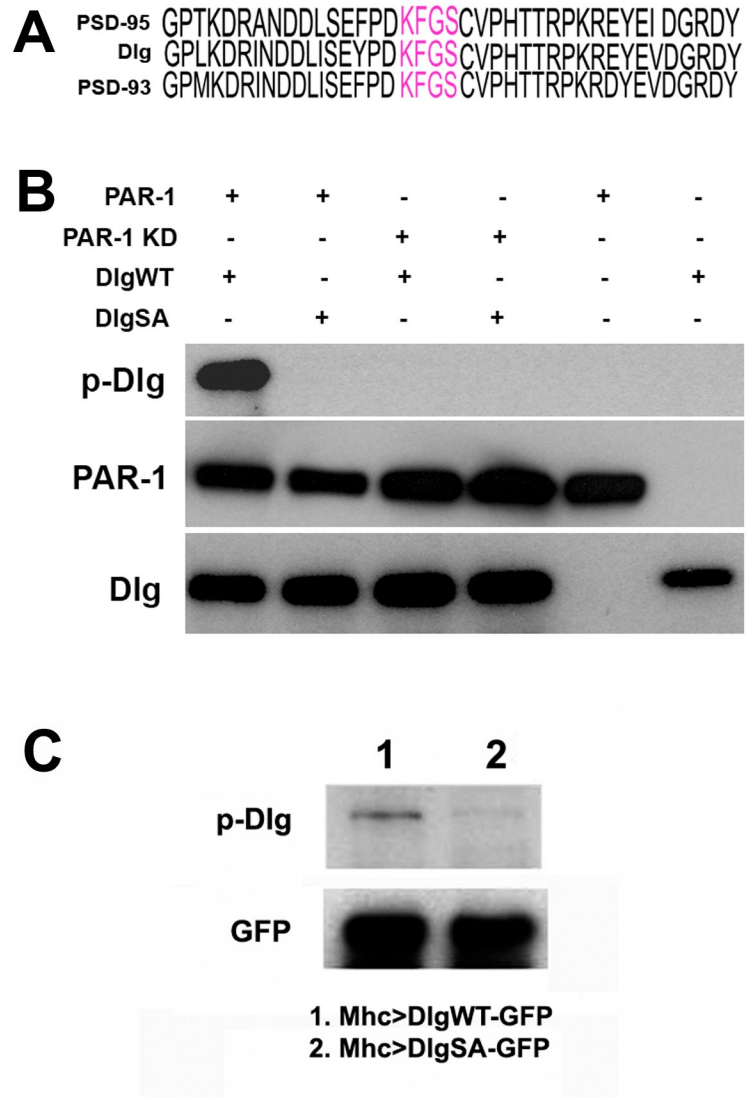


**Figure S8**. Assessment of the specificity of the p-Dlg antibody.

(A) Sequence alignment of the "KFGS" motif and its flanking amino acid residues in PSD-95 (mouse), PSD-93 (mouse), and Dlg (fly). The S797 residue and its flanking amino acids are highly conserved.

(B) Testing the specificity of p-Dlg antibody in heterologous cells. To generate the constructs for expression in HEK293T cells, The DlgWT and DlgS797A mutant cDNAs were cloned in-frame into a *pcDNA3* expression vectors harbouring a Flag tag in the N-

terminus. Similarly, the PAR-1WT and PAR-1 KD cDNAs tagged with a myc epitope were cloned into *pcDNA3* vector. Different combinations of PAR-1 and Dlg constructs were transacted into HEK293T cells using Lipofectamine Reagent (Invitrogen). 48 hrs after transfection, cell lysates were immunprecipated with anti-Dlg and the immunocomplex probed with anti-p-Dlg. Only when wild type PAR-1 and wild type Dlg were co-transfected that Dlg became phosphorylated at S797. The experiment was repeated twice and similar results were obtained.

(C) Western blot analysis of body-wall muscle extracts prepared from *Mhc>DlgWT-GFP* and *Mhc>DlgSA-GFP* animals. When equal amounts of DlgWT-GFP and DlgSA-GFP fusion proteins were probed with p-Dlg antibody, DlgWT-GFP was preferentially recognized.

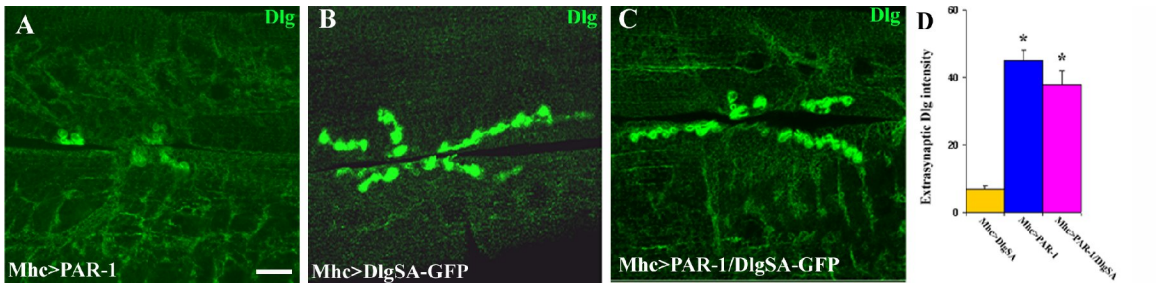


**Figure S9**. Analysis of the distribution patterns of endogenous Dlg in *Mhc>PAR-1* (A), *Mhc>DlgSA-GFP* (B), and *Mhc>PAR-1/DlgSA-GFP* (C) NMJs. Note that in *Mhc>PAR-1/DlgSA-GFP* animals, a large proportion of endogenous Dlg was still mislocalized by the overactivation of PAR-1, even though the SSR and synapse structures were restored to nearly normal by DlgSA-GFP. (D) Statistical analysis of the relative extrasynaptic levels of endogenous Dlg among the three genotypes. The differences between *Mhc>DlgSA-GFP* (n=21) and *Mhc>PAR-1* (n=19) and between *Mhc>DlgSA-GFP* (n=21) and *Mhc>PAR-1/DlgSA-GFP* (n=27) are statistically significant ($P<0.001$). Scale bar: 5 μm.

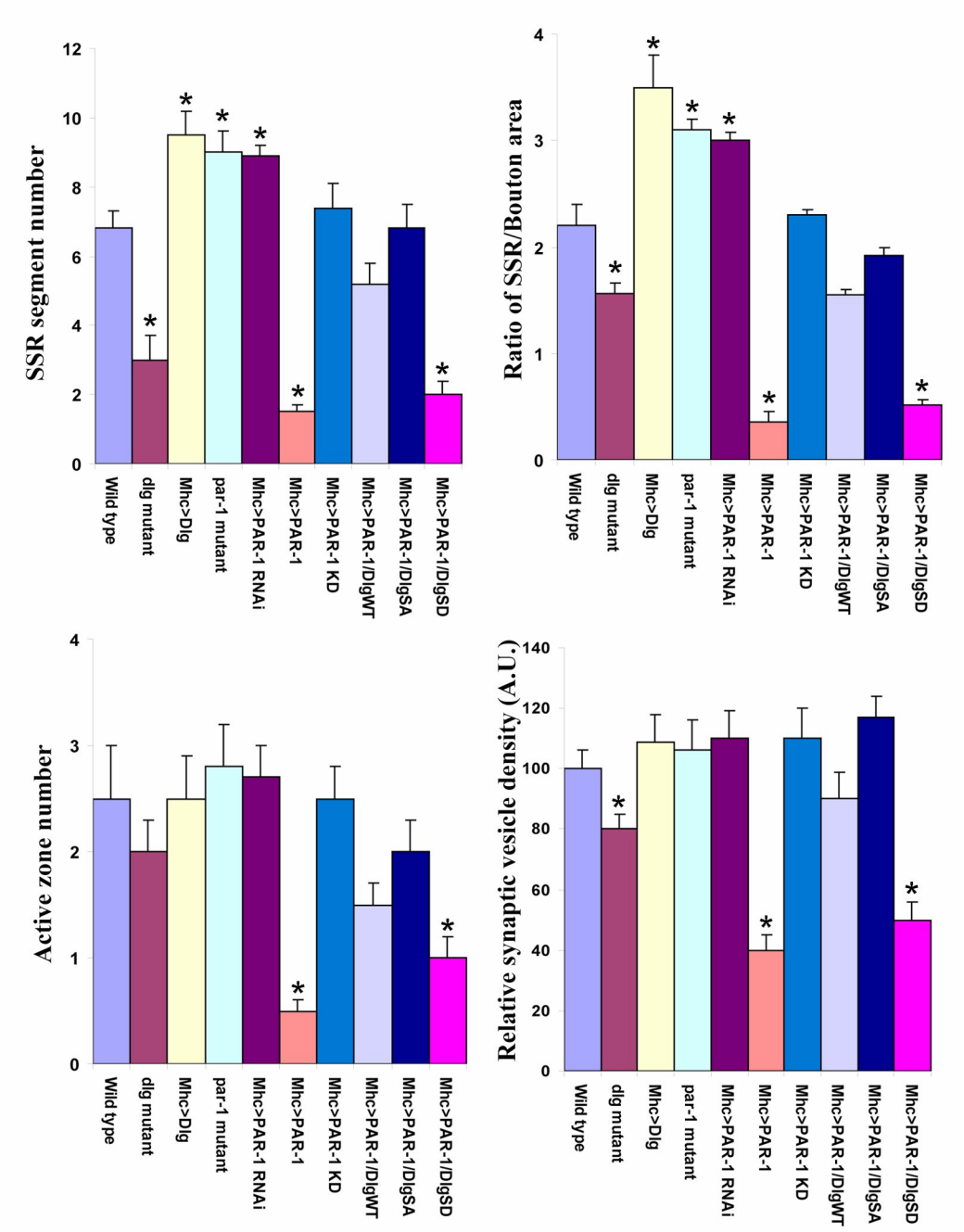


**Figure S10**. Quantitative analysis of the alterations of synaptic ultrastructures caused by PAR-1 loss of function and overexpression and the rescue of PAR-1 overexpression effect by DlgWT-GFP and DlgSA-GFP. EM micrographs of wild type (n=7, 66 midline cross-sections), *dlg* mutant (n=8, 70 sections), *Mhc>Dlg* (n=9, 71 sections), *par-1*$^{\Delta 16}$*/par-1*$^{9A}$ mutant (n=10, 70 sections), *Mhc>PAR-1 RNAi* (n=7, 62 sections), *Mhc>PAR-1* (n=10, 70 sections), *Mhc>PAR-1 KD* (n=9, 85 sections), *Mhc>PAR-1/DlgWT-GFP*

(n=10, 78 sections), *Mhc>PAR-1/DlgSA-GFP* (n=10, 65 sections), and *Mhc>PAR-1/DlgSD-GFP* (n=10, 72 sections) were analyzed for SSR segment number, active zone number, SSR area vs. bouton area ratio, and relative synaptic vesicle density (A.U: arbitrary unit). Asterisks indicate statistical significance in Student's t test (P<0.01) when compared to the wild type controls.

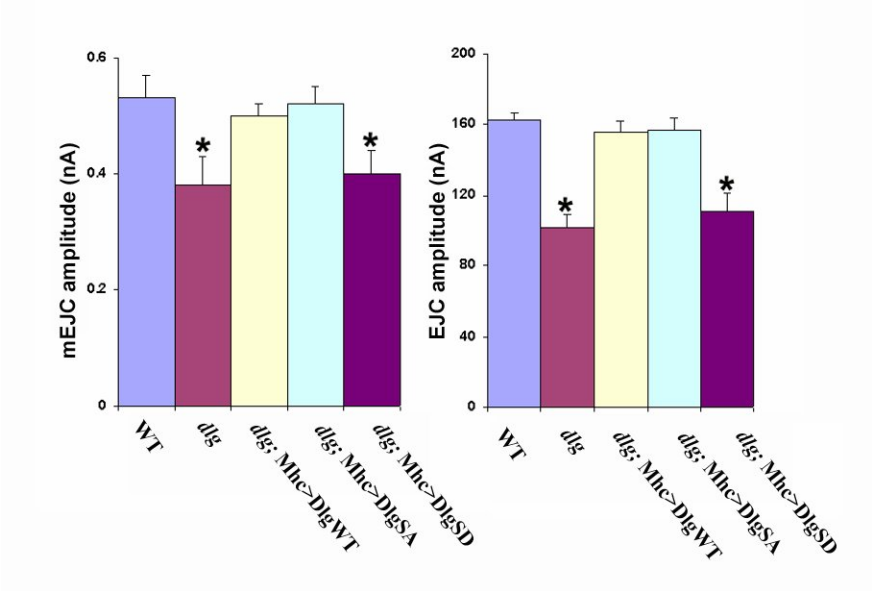


**Figure S11**. Electrophysiological analysis showing rescue of $dlg^{X1-2}$ mutant synaptic transmission defects by DlgWT-GFP, DlgSA-GFP, and DlgSD-GFP. mEJC amplitude and EJC amplitude of wild type (n=20), $dlg^{X1-2}$ mutant (n=26), $dlg^{X1-2}$; *Mhc>DlgWT-GFP* (n=27), $dlg^{X1-2}$; *Mhc>DlgSA-GFP* (n=29), and $dlg^{X1-2}$; *Mhc>DlgSD-GFP* (n=25) animals were compared. Asterisks indicate statistical significance (P<0.01) when compared to the wild type controls in Student's t test.